International Journal of Heat and Mass Transfer 246 (2025) 127037

Contents lists available at ScienceDirect

International Journal of Heat and Mass Transfer

journal homepage: www.elsevier.com/locate/hmt

Interfacial effects on thermal conductive properties in PEEK composites

Siqin Liu [a], Yanan Zhang [b], Xin Yan [a,c,*], Wuxiang Zhang [a,c], Xilun Ding [a,c]

[a] School of Mechanical Engineering and Automatic, Beihang University, Beijing, 100191, China
[b] Tieke Zongheng (Tianjin) Technology Development Co., Ltd., Tianjin, 301709, China
[c] Ningbo Institute of Technology, Beihang University, Ningbo, 315832, China

ARTICLE INFO

Keywords:
PEEK composites
Thermal properties
Interfacial thermal resistance (ITR)
Molecular dynamics

ABSTRACT

Polyether ether ketone (PEEK) is a high-performance thermoplastic composite matrix material renowned for its exceptional mechanical properties and thermal stability, making it highly suitable for high-temperature applications. However, the interfacial thermal resistance (ITR) at the micro-scale interfaces between the polymer matrix and fillers in PEEK composites, which significantly impacts heat transfer, has not been extensively explored. In this study, we investigated the interfacial thermal properties of PEEK composites with various filler materials using molecular dynamics simulations and the theoretical model. Our results indicate that PEEK/SiO_2 composites exhibit superior interfacial thermal properties compared to other selected materials, while PEEK/SiC composites display the highest interfacial thermal resistance. Due to the effect of ITR, the introduction of fibers may not always improve the effective thermal conductivity of the composite. The effect of ITR is also related to the filler size and shape. Reducing the size of the filler magnifies the effect of ITR, and there is a critical filler length which could be used to distinguish between the positive and negative thermal effects of introducing fillers. Our research illustrates a multiscale modeling approach to evaluate the ITR effect on the thermal properties of PEEK composite, which could be extended to other composite systems. The findings could benefit the multiscale modeling of composite manufacturing and the micro-structure design of composites with consideration of thermal management.

1. Introduction

Poly ether ether ketone (PEEK) composite has attracted considerable attention across various industries including aerospace, automotive, medical, and electronics, due to their exceptional material properties. PEEK is recognized as a high-performance polymeric material that exhibits excellent mechanical properties, high thermal stability, good chemical resistance, and biocompatibility [1,2]. It can be reinforced with various fillers, including graphene [3], SiC [4,5], SiO_2 [6,7], etc., to produce composites with different properties [1,8,9].

For thermoplastic resin, such as PEEK, the efficiency of heat transfer during manufacturing would directly influence the thermal distribution within the material and the temperature history during processing. These factors affect both the phase transition behaviors and the mechanical response to local temperature variations, which determine the overall quality of the final product [10]. Additionally, as thermal management becomes increasingly important for high-temperature applications, such as aircraft components [11] and electronic devices [12], the heat dissipation capability of composites has become a key focus, especially for PEEK composites [9]. Within the PEEK matrix, usually, the incorporation of highly thermally conductive fillers can not only increase the mechanical properties but also enhance the thermal properties of the composite. However, it also introduces numerous interfaces between the polymer matrix and the fillers, which can generate interfacial thermal resistance (ITR) [13]. The presence of ITR can impede the efficient transport of heat within the material, thereby limiting the overall thermal performance [13,14]. This interfacial effect is particularly pronounced in composites with poor filler/polymer interaction or those containing nanoscale fillers that dramatically increase the interfacial area [12]. Achieving the optimal performance of composite materials necessitates a comprehension of their thermal behaviors, particularly the effects of ITR, which are essential for both the optimization of the manufacturing process and the micro-structural design of the composites.

The ITR has been extensively investigated in numerous polymeric nanocomposites and is often calculated using molecular dynamics simulation [3,15–21], which offers valuable insights into the heat transfer mechanism at the atomistic level [11,22,23]. For instance, Wu et al. obtained the ITR in four different types of PEEK/graphene nanocomposites using MD simulation, and analyzed the influence of varying functional groups [3]. Additionally, multiple studies have investigated

* Corresponding author at: School of Mechanical Engineering and Automatic, Beihang University, Beijing, 100191, China.
E-mail address: yan_xin@buaa.edu.cn (X. Yan).

https://doi.org/10.1016/j.ijheatmasstransfer.2025.127037
Received 8 December 2024; Received in revised form 28 February 2025; Accepted 27 March 2025
Available online 16 April 2025

Nomenclature

D	Filler diameter
D_S	Phonon density of states in the composite
f	Filler volume fraction
G	Interfacial thermal conductance
J_z	Heat flux in the z-direction
K_{eff}	Effective thermal conductivity of composite
K_f	Thermal conductivity of the filler material
K_m	Thermal conductivity of the polymer matrix
L	Filler length
L_k	Kapitza length on the interface
M	Correlation factor in phonon density of states between different atom types
P	Filler aspect ratio
R_I	Interfacial thermal resistance
T	Temperature

the effect of ITR on the thermal transport efficiency of composites. These investigations have provided new strategies to enhance thermal management, taking into account other important factors such as filler fraction, filler orientation, and filler shapes [24,25]. However, a gap remains in the literature regarding the interfacial effects on the thermal properties of PEEK composites, particularly concerning varying filler types such as inorganic fillers like silicon carbide and silicon dioxide [26]. These fillers exhibit varying shapes (such as fibers, spherical, flake) and sizes (from nanometer to micrometer) [27,28], which can significantly influence the thermal properties of the composites. Therefore, the absence of a comprehensive understanding of their thermal behavior, including the effects of ITR, may hinder the optimization of composite performance in advanced applications.

This work aims to present comprehensive analyses that investigate the impact of ITR on the thermal properties of PEEK composites containing different types of fillers. We begin with a MD simulation to assess the interfacial thermal properties between filler materials and polymer matrices in PEEK composites, including PEEK/graphene, PEEK/SiO_2, and PEEK/SiC. Based on the results from our MD simulation, we calculated the effective thermal conductivities of the composites using an effective medium theory model, considering various filler volume fractions, sizes, and shapes. Our multiscale model and analysis could provide valuable insights into the impact of interfacial thermal resistance on the thermal behavior of composites, which can contribute to enhancing thermal properties and improving the accuracy of thermal simulations.

2. Models and simulations

2.1. Atomistic model construction

Various atomistic models were constructed to represent the interfacial structure of PEEK composites, including PEEK/graphene, PEEK/SiO_2, and PEEK/SiC, as depicted in Fig. 1. Initially, the amorphous PEEK polymer is synthesized from ether ether ketone (EEK) monomers. This particular model features 15 polymer chains, with each chain being composed of 15 EEK units. The PEEK polymer has a density of 1.30 g/cm^3 [29] and contains a total of 7680 atoms within a simulation box measuring 42.6 Å × 49.2 Å × 39.5 Å. Subsequently, the initial polymer structure was optimized on the LAMMPS platform [30] following a series of relaxation procedures to achieve equilibrium, including microcanonical (NVE) for 100 ps, and canonical (NVT) at 300 K for 1 ns. The time step was set to 1 fs, and periodic boundary conditions were applied in all three spatial directions of the model.

Graphene sheets, α-SiO_2, and β-SiC were utilized as filler material that can also represent the nanostructure of carbon fiber [31], glass fiber [32,33], and SiC fiber [34]. The graphene exhibited a well-ordered structure, comprising seven layers and a total of 5600 atoms, within a simulation box of dimensions 42.6 Å × 49.2 Å in-plane and 20.0 Å out-of-plane (as shown in Fig. 1b). The α-SiO_2 was constructed from a crystalline silica structure containing 2772 atoms. Following a quenching process, as described in [33], the structure was transformed into an amorphous structure. Subsequently, an equilibrium isothermal–isobaric (NPT) process was applied to the α-SiO_2 to achieve a simulation box dimension of 42.6 Å × 49.2 Å × 20.0 Å and a density of 2.20g/cm^3 at 300 K.

Three types of symmetric composite structures were constructed by combining the polymer and filler structures, including PEEK/graphene, PEEK/SiO_2, and PEEK/SiC. Initially, a geometric optimization was performed on the structures using conjugate gradient energy minimization. Subsequently, the structures underwent a series of equilibrium and to form the proper contact between the matrix and the fillers. The equilibrium process involved simulations under NVE conditions for at least 100 ps, under NVT conditions for at least 1 ns, and a hot compression procedure under NPT conditions for at least 100 ps. Periodic boundary conditions were applied in all three spatial directions. The final box size was approximately 43.0 Å × 49.0 Å × 120.0 Å with variations observed among different composites. Additionally, the final density of PEEK matrix was maintained at 1.30 g/cm^3, which is consistent with the experimental testing [29].

To capture the interactions between different types of atoms, a hybrid potential was utilized in the composite systems. The polymer consistent force field (PCFF) [35] was employed to model the molecular behavior within the PEEK polymer material [36], include both valence and non-bond interaction. The valence interaction consists of the bond stretching, angle bending, and dihedral torsion, while the non-bond interaction describes the van der Waals and Coulombic forces among articles. For the covalent bonding and non-bonding interaction of fillers, the adaptive intermolecular reactive empirical bond order (AIREBO) potential [37] was applied to simulate the graphene [15,36], while the Tersoff potential was used to describe SiO_2 [38] and SiC [39] fillers. Furthermore, across the interface between the polymer and filler, the interaction between atoms is assumed to be governed by van der Waals forces. This interaction is described using a 6/9 Lennard-Jones potential, with pair coefficients modified according to the sixth-power mixing rule [40,41]. The detailed formulas and associated parameters are provided in the supplementary note 1.

2.2. Thermal properties calculation

A series of non-equilibrium molecular dynamics (NEMD) simulations were conducted to calculate the thermal properties of composite systems [22]. Initially, the composites were placed within a Berendsen thermostat at a fixed temperature of 300 K for sufficient time to eliminate non-negligible temperature gradients within the material. Then the composites were subjected to NVE ensembles, where a specific amount of heat was added and extracted from the reservoir regions at regular intervals, as illustrated in Fig. 2. Periodic conditions were applied in all three spatial directions. The induced heat flux J_z of the entire system can be obtained by:

$$J_z = \frac{\Delta Q_z}{2A}, \tag{1}$$

where ΔQ_z represents the rate of heat addition in the heat source or the rate of heat abstraction in the heat sink, which is set as a constant value of 0.01 kcal mole^{-1} fs^{-1} in the composite systems. Additionally, A denotes the cross-sectional area of the simulation box.

Over a period of time, a steady temperature distribution was developed within the system, which was then used for the calculation of the thermal properties of the materials. Specifically, the thermal

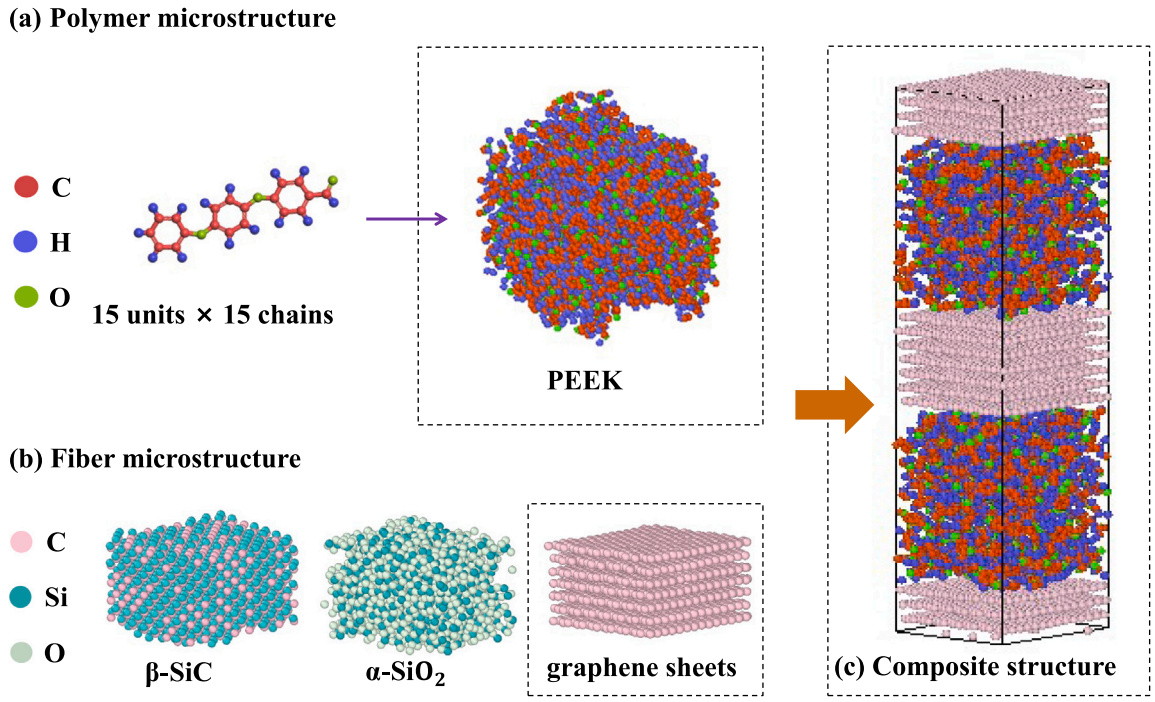

Fig. 1. Atomistic model of (a) PEEK, (b) fibers and (c) composite system.

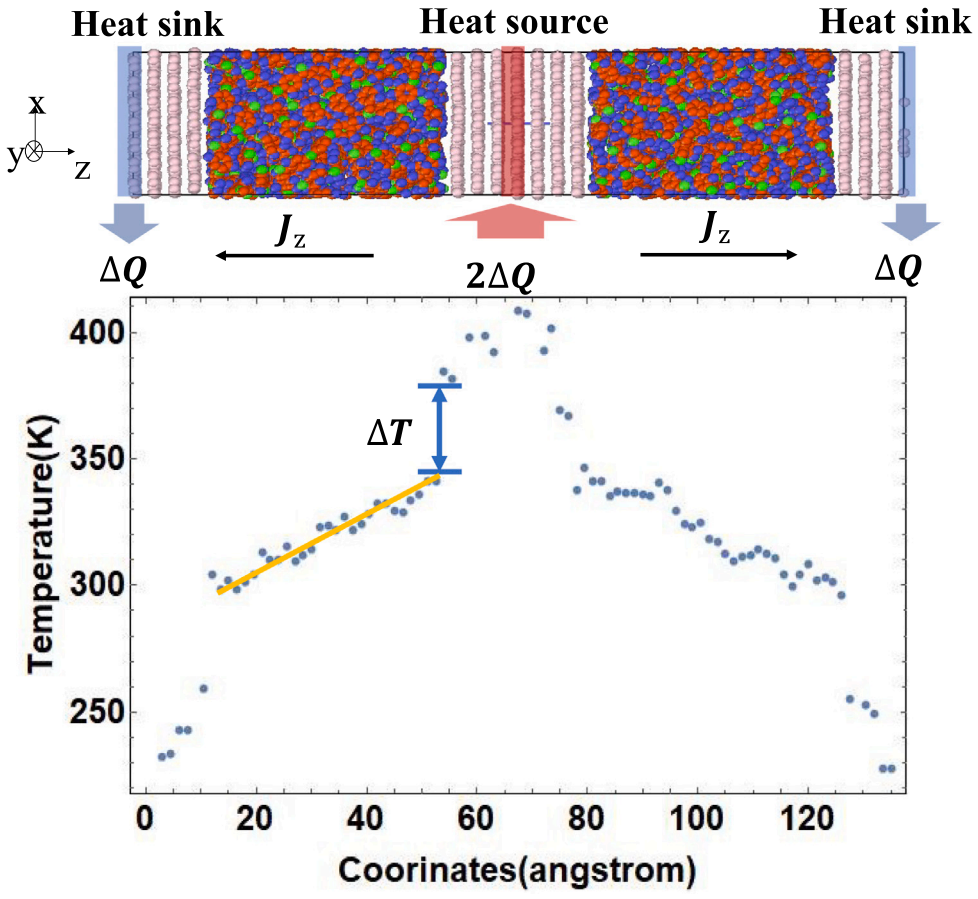

Fig. 2. Schematic diagram of heat transport and temperature distribution in NEMD.

conductivity of the polymer matrix in the z-direction can be determined by:

$$k = -\frac{J_z}{\partial T/\partial z}, \tag{2}$$

where $\partial T/\partial z$ refers to the temperature gradient inside polymers. Meanwhile, the interfacial thermal conductivity G and the interfacial thermal resistance R_I are defined as:

$$G = \frac{J_z}{\Delta T}, R_I = \frac{\Delta T}{J_z} = \frac{1}{G}, \tag{3}$$

where ΔT represents the temperature difference between the polymer and filler.

2.3. Validation of thermal conductivity calculation for PEEK polymer

A pure PEEK polymer model was built to investigate its thermal conductivity at the room temperature of 300 K. This model has a dimension of 42.6 Å × 49.2 Å × 79 Å with a density of 1.3 g/cm^2 [29]. The thermal conductivity of the PEEK polymer was calculated to be 0.3 $Wm^{-1}K^{-1}$, which aligns closely with the value of 0.29 $Wm^{-1}K^{-1}$ reported by Nikonovich et al. for commercial PEEK [42]. This validates the suitability of the simulation model as well as the potential for estimating the thermal properties of PEEK.

3. Results and discussion

3.1. Comparison of the interfacial thermal conductivity

The interfacial thermal conductivity of PEEK composites at 300 K was determined for three distinct filler materials: graphene, SiO_2, and SiC. For each composite, we consider three different configurations of the amorphous structure, including the polymer and the SiO_2. These configurations have statistically similar systems, with the same constraints and temperature.. The result is presented in Fig. 3(b). Among all the composite materials evaluated, PEEK/SiO_2 exhibits the most favorable interfacial thermal transport behavior, with an average interfacial thermal conductivity value of 113.3 $MWm^{-2}K^{-1}$. This value is about 6.3 times higher than the average interfacial thermal conductivity value of PEEK/SiC, which is 18.0 $MWm^{-2}K^{-1}$. Additionally, the interfacial thermal conductivity of PEEK/graphene measures approximately 45.3 $MWm^{-2}K^{-1}$, roughly 2.5 times larger than that of PEEK/SiC. The effects of filler length and polymer chain length on the interfacial thermal conductivity were also investigated. Our finding indicates that the material does exhibit a size effect to varying degrees. However, due to the scale limitations of atomistic modeling, it is challenging to precisely quantify the exact size effect. Nevertheless, these effects do not significantly impact the major conclusions we have drawn. Therefore, we neglected the size effect in our further calculations. Detailed illustrations can be found in the supplementary note 2.

3.2. Phonon analysis of the interfacial thermal properties

To understand the notable differences in the interfacial thermal properties observed among these PEEK composites, the phonon density of states (PDOS) analysis was applied. This approach provides insights into the heat transport mechanisms at the nanoscale between the amorphous polymer and the filler materials [15,20,43,44]. The PDOS can be obtained by the following equation [44]:

$$D_S(f) = \int_0^\tau \frac{\langle \mathbf{v}(t)\mathbf{v}(0)\rangle}{\langle \mathbf{v}(0)\mathbf{v}(0)\rangle} \cos(2\pi f t)dt, \tag{4}$$

where $D_s(f)$ represents the PDOS of atoms at the frequency of f, the terms $\langle \mathbf{v}(t)\mathbf{v}(0)\rangle$ and $\langle \mathbf{v}(0)\mathbf{v}(0)\rangle$ denote the velocity–velocity autocorrelation functions. $\mathbf{v}(0)$ is the atom velocity at the initial time and $\mathbf{v}(t)$ is the atom velocity at the time t. In this simulation, the velocity data was collected over a period of 100 ps at an NVT equilibrium state of 300 K.

The PDOS of the PEEK/SiC composite within the frequency range of 0 to 50 THz is depicted in Fig. 4. As shown in Fig. 4(a), representative regions within the composite are denoted using circled numbers 1 through 5. In Fig. 4(b), the uppermost panels display the unique PDOS characteristics of SiC atoms, with carbon (C) on the left and silicon (Si) on the right of the corresponding regions. The light green areas, purple lines, and blue lines correspondingly represent the PDOS of filler atoms from positions away from the interface to those at the interface (spanning regions 1 to 3). It is noticeable that from regions 1 to 3, the peak frequency of both carbon and silicon atoms shifts towards lower frequencies at the interface, as indicated by the black arrows. This shift reflects the impact of interfacial interactions on the movement of filler atoms. The central panels illustrate the movements of polymer and filler atoms at the interface (region 3), with the orange lines representing PEEK carbon atoms and the blue lines representing SiC atoms. It can be seen that the predominant frequencies of amorphous polymer carbon atoms cover a broad spectrum of 0 ~ 50 THz. In contrast, as highlighted with light blue areas, the carbon atoms in the SiC filler occupy a narrower frequency range of 20 THz to 30 THz, and the silicon atoms in SiC span from 0 to 30 THz. This significant discrepancy in the dominant phonon frequencies at the interface between SiC atoms and PEEK carbon atoms indicates markedly different phonon modes. Such differences in phonon behavior lead to increased phonon scattering. This in turn results in an interfacial thermal resistance, affecting the heat transfer between the polymer and filler molecules. The lower panel showcases the PDOS of PEEK carbon atoms across the interface region (region 3 with orange lines) extending to the bulk regions within PEEK (region 4 with green lines and region 5 with a light blue area). It shows that the peak frequency of PEEK carbon atoms in the range of 0 to 10 Hz shifts slightly towards higher frequencies (from regions 5 to 3). This transformation is due to the interaction of polymer atoms with filler atoms at the interface.

Although there are distinct vibration modes in PEEK/SiO_2 and PEEK/graphene, they exhibit similar behavior to those in PEEK/SiC and will not be extensively discussed individually. These materials also undergo a shift in phonon vibration modes from the bulk region to the interface region. Besides, there is a noticeable mismatch in the movements of polymer carbon atoms and diverse filler atoms at the interface, as illustrated in Fig. 5(a). The panels from top to bottom represent the behavior of PEEK/SiC, PEEK/SiO_2, and PEEK/graphene, respectively. Recognizing that the coupling of polymer and filler phonon patterns in the low-frequency domain governs the efficiency of heat transport across the interface [22], the frequency spectrum is categorized into three segments for analysis [45]: low-frequency domain (0 ~ 15 THz in light orange), middle-frequency domain (15 ~ 30 THz in light blue), and high-frequency domain exceeding 30 THz (in white). The varying phonon patterns of the filler atoms demonstrate different levels of overlap with the PEEK carbon atoms. In the PEEK/SiC composites (shown in the top panel), the carbon atoms in SiC fillers (the blue line in the left plot) predominantly concentrate in the middle-frequency domain, indicating a limited contribution to thermal transport across the interface. In the middle panels, amorphous SiO_2 atoms (purple solid line for C in the left plot and purple dashed line for Si in the right plot) cover the entire frequency range from 0 to 50 Hz without sharp peaks, demonstrating a better match with PEEK phonons (orange lines) than PEEK/SiC. Furthermore, in the lower panel, a significant number of graphene atoms (green line) lies in the frequency domain below 20 THz, showing an effective coupling with the polymer atoms at the low-frequency domain. To quantitatively access the coupling in composite interfacial atoms, a correlation factor (M) is defined to calculate the PDOS overlap area as [46]:

$$M = \frac{\int_0^{f_c} D_A(f)\cdot D_B(f)df}{\int_0^{\infty} D_A(f)df \cdot \int_0^{\infty} D_B(f)df}, \tag{5}$$

where D_A and D_B refer to the PDOS of two different atom types A and B, and f_c refers to the cutoff frequency. A higher value of M indicates a better match in the PDOS.

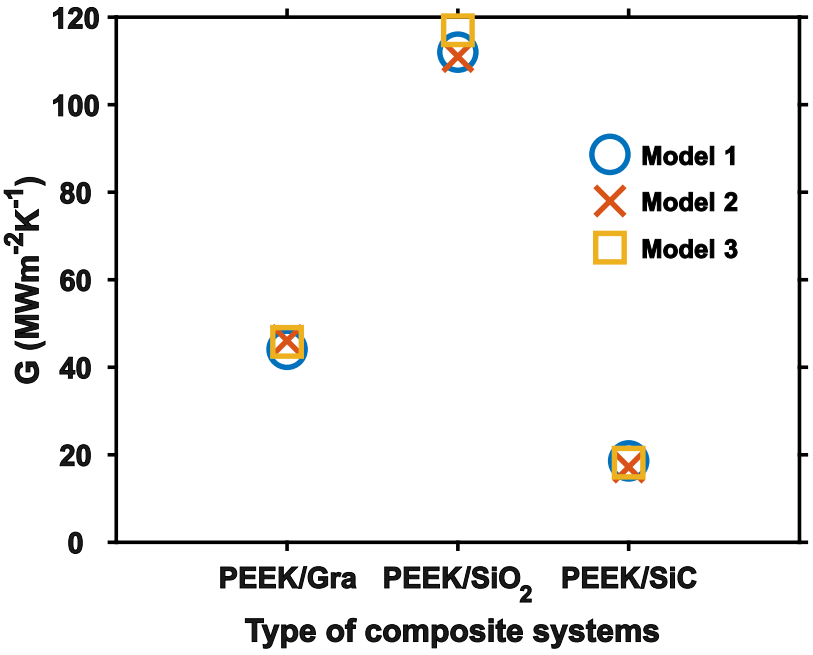

Fig. 3. Interfacial thermal conductivity of PEEK composites.

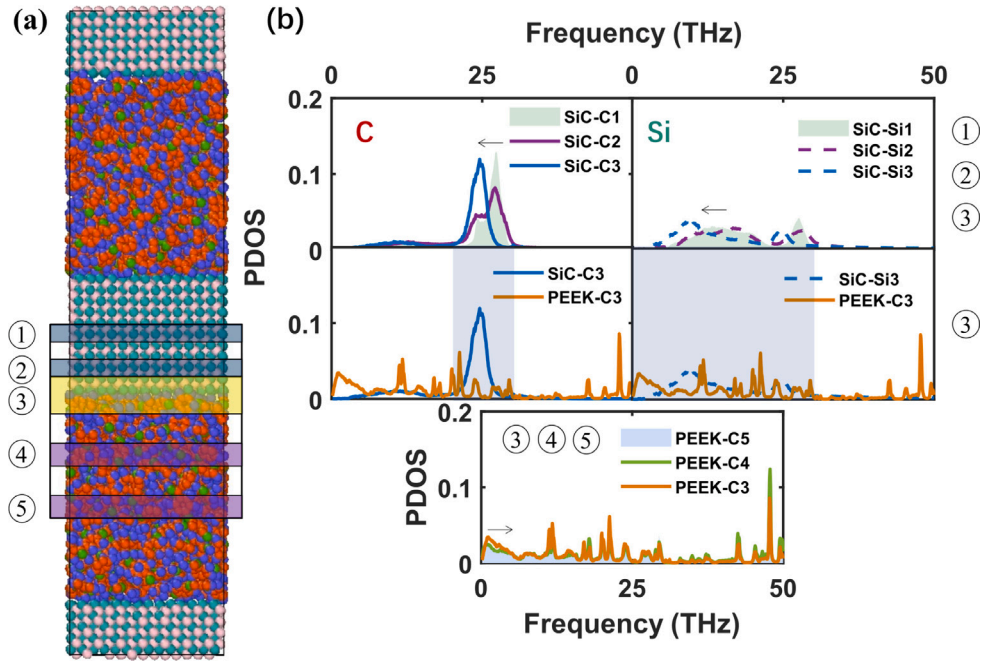

Fig. 4. (a) The atomistic model of PEEK/SiC composite with labeled regions. Regions 1 to 3 contain filler atoms, while regions 3 to 5 consist of polymer atoms. Region 3 is the interface containing both filler and polymer atoms. (b) PDOS of PEEK/SiC composite in various regions. The panels from top to bottom depict the PDOS for: SiC filler atoms (carbon on the left and silicon on the right), SiC filler atoms and PEEK carbon atoms in the interface region, and PEEK carbon atoms in the corresponding regions (labeled with circled numbers). The light blue areas in the central panel highlight the predominant frequencies of the carbon and silicon atoms of the SiC filler within the interface (region 3). The black arrows depict the peak frequency shift of the PDOS from the interior fiber (or polymer) regions to the interface regions. (For interpretation of the references to color in this figure legend, the reader is referred to the web version of this article.)

The variation of M with frequency for interfacial atoms in different PEEK composites is shown in Fig. 5(b). Given the predominant effect of phonon overlap in the low-frequency region as opposed to the mid-frequency and high-frequency regions on interfacial heat transport, scrutiny of the low-frequency region reveals that the correlation factor M in PEEK/SiO_2 (purple lines) consistently exceeds that in PEEK/graphene (green line) and PEEK/SiC (blue lines). Consequently, PEEK/SiO_2 demonstrates superior performance in interfacial heat transfer compared to PEEK/graphene and PEEK/SiC composites. In the scenario of PEEK/SiC, the limited correlation factor value of PEEK carbon atoms with SiC carbon atoms (blue dashed line) indicates the insufficient coupling of these atoms, which leads to a reduced value of interfacial thermal conductivity as shown in Fig. 3.

3.3. Effective thermal conductivities of composites

To analyze the influence of the interfacial thermal resistance on the thermal behaviors of the composite structures, Nan's effective medium

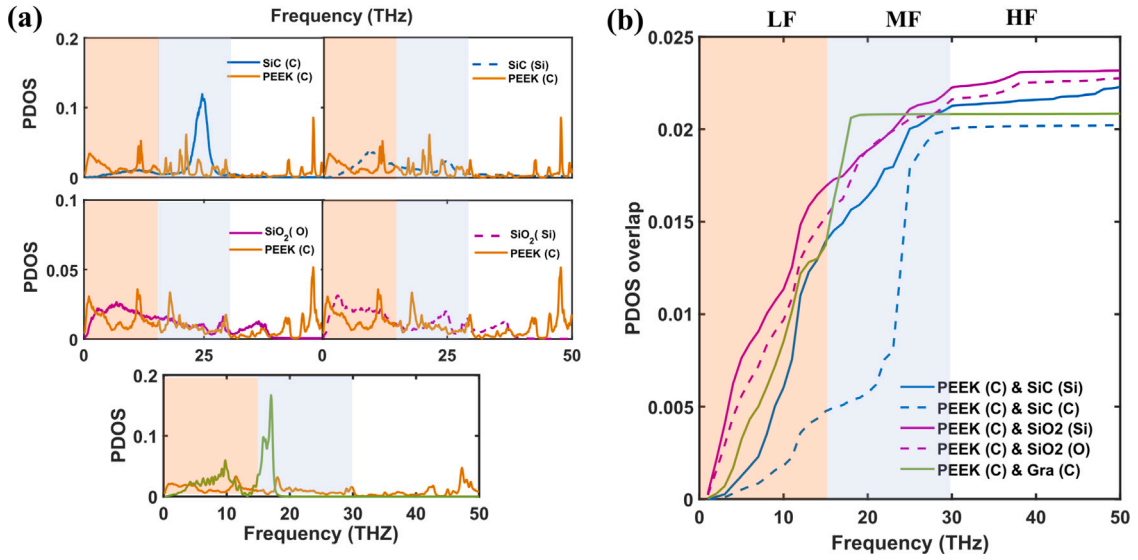

Fig. 5. Phonon characteristics at interfacial regions of PEEK composites: (a) PDOS of PEEK composites at the interface (top to bottom: PEEK/SiC, PEEK/SiO_2, PEEK/graphene); (b) the correlation factor (M) of PDOS for PEEK composites. The frequency spectrum is divided into three segments: the low-frequency domain (LF in light orange), the middle-frequency domain (MF in light blue), and the high-frequency domain (HF in white). (For interpretation of the references to color in this figure legend, the reader is referred to the web version of this article.)

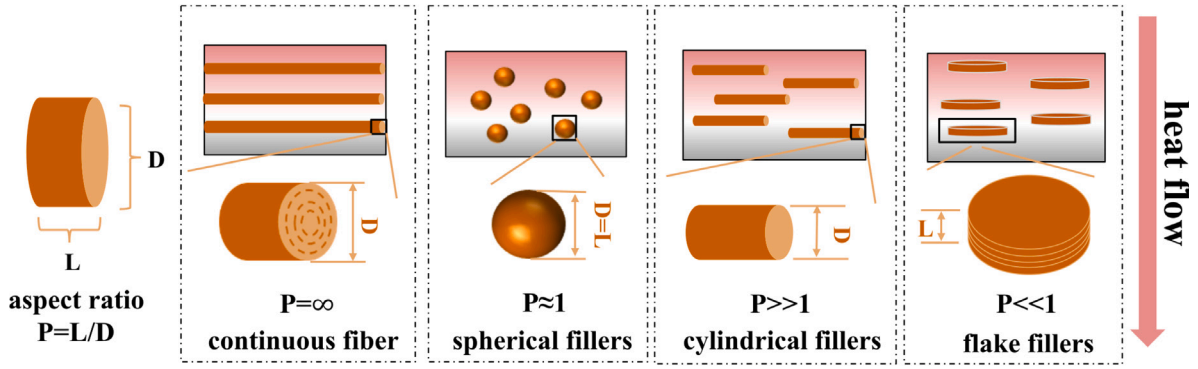

Fig. 6. Illustration of different filler types and the heat flow direction under consideration.

theory [47] was employed to calculate the effective thermal conductivities (K_{eff}) of the composites with various filler types, including continuous fiber, spherical fillers, flake fillers, and cylindrical fillers, as illustrated in Fig. 6. The type of fillers was characterized by the fiber aspect ratio P, which represents the ratio of filler length L to diameter D. In continuous fibers, the length markedly exceeds the diameter ($P = \infty$), with diameters typically in the microscale range. Specifically, carbon fibers were assumed to have a circumferential arrangement of graphene sheets in their cross-section [48]. Fillers with P values close to 1 are classified as spherical fillers. When the length of the filler is much less than the diameter, the filler is identified as a flake filler. Conversely, when the P value significantly surpasses unity ($P \gg 1$), the filler falls under the category of cylindrical fillers.

When calculating K_{eff}, it was assumed that the fillers aligned in the same direction, and heat flowed along the direction corresponding to the shorter dimension of the filler: the length direction for flake fillers, the diameter direction for cylindrical fillers, and with no distinct direction for spherical fillers, as shown in Fig. 6. This configuration allows heat to pass through a substantial number of interfaces, thereby highlighting the interfacial effects. In all cases, heat propagation occurred in the out-of-plane direction for the graphene sheets, which exhibits the weakest heat transfer efficiency. Additionally, we assume a dispersed distribution of the filler materials within the resin and neglect the filler–filler interactions, such as the ITR between fillers [14].

The effective thermal conductivity of the composite is then determined in the length (K_{eff}^{L}) or the diameter (K_{eff}^{D}) directions of the fillers [47]:

$$K_{\text{eff}}^{i} = K_{\text{m}} \frac{1 + f\beta_i(1 - L_i)}{1 - f\beta_i L_i} \quad \text{for} \quad i \in \{L, D\}, \tag{6}$$

with

$$\beta_i = \frac{K_i^c - K_{\text{m}}}{K_{\text{m}} + L_i(K_i^c - K_{\text{m}})}, \tag{7}$$

where

$$K_i^c = \frac{K_{\text{f}}}{1 + \gamma L_i K_{\text{f}}/K_{\text{m}}}. \tag{8}$$

Here, the index i indicates the filler length ($i = L$) or the filler diameter ($i = D$) direction in K_{eff} calculation. The variable f denotes the volume fraction of the filler. The term K_{m} represents the thermal conductivity of the resin material. K_{f} is the thermal conductivity of the filler material. The parameters L_D and γ depend on the aspect ratio p, and $L_L = 1 - 2L_D$. When $p > 1$, there is:

$$L_D = \frac{p^2}{2(p^2 - 1)} - \frac{p}{2(p^2 - 1)^{3/2}} \cosh^{-1} p, \tag{9}$$

$$\gamma = \frac{(2 + 1/p)K_{\text{m}}}{GD}. \tag{10}$$

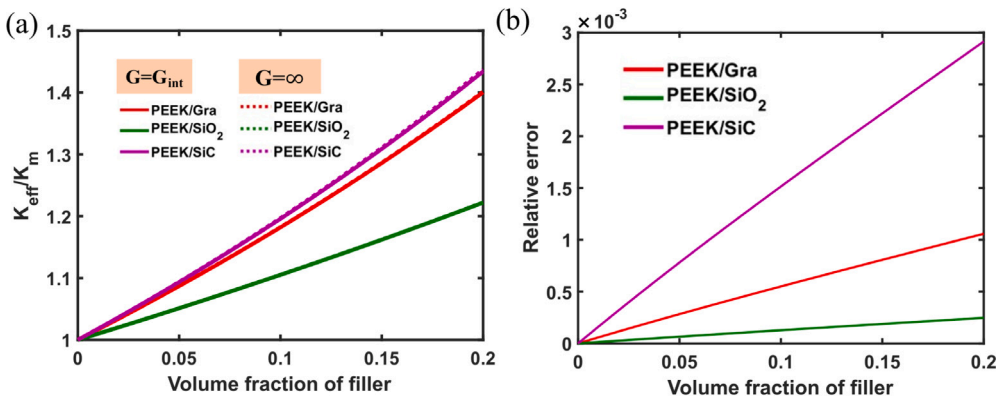

Fig. 7. The influence of interfacial thermal conductivity on composites reinforced with continuous carbon fiber, glass fiber, and SiC fiber: (a) The $K_{\text{eff}}/K_{\text{m}}$ ratio of composites with varying volume fractions of the fillers. (b) The relative error in K_{eff} with varying volume fractions of the fillers. (For interpretation of the references to color in this figure legend, the reader is referred to the web version of this article.)

When $p < 1$, there is:

$$L^D = \frac{p^2}{2(p^2-1)} + \frac{p}{2(1-p^2)^{3/2}} \cos^{-1} p, \tag{11}$$

$$\gamma = \frac{(1+2p)K_{\text{m}}}{GL}. \tag{12}$$

As p approaches 1, L_D tends to 1/3. In these equations, G refers to the interfacial thermal conductivity. We note that NAN's theory can calculate the effective thermal conductivity for composites with both aligned and randomly distributed fillers. In this work, we focus only on the aligned case. More discussions regarding the randomly distributed case can be found in [47].

In order to uncover the effects of the interface on the effective thermal conductivities of the composites, two distinct scenarios were examined: one that includes the consideration of interfacial thermal resistance ($G = G_{\text{int}}$) and another one that assumes an ideal interface with no thermal resistance, where the interfacial thermal conductivity is effectively infinite ($G = \infty$). The disparity between these two scenarios highlights the significance of incorporating interfacial thermal resistance, which was quantified through the relative error R using the following equation:

$$R = \frac{K_{\text{eff}}(G=\infty) - K_{\text{eff}}(G=G_{\text{int}})}{K_{\text{eff}}(G=\infty)}. \tag{13}$$

In this equation, the effective thermal conductivity K_{eff} is calculated through substituting the atomistic simulation results into NAN's theory. A higher value of R leads to increased overestimation in the prediction of K_{eff} when the interfacial thermal resistance is neglected.

In the calculation of K_{eff} and R, all the significant material properties K_{m}, K_{f}, and G were calculated from our MD simulations. Specifically, the K_{m} of pure PEEK resin was determined to be 0.3 $\text{Wm}^{-1}\text{K}^{-1}$. The values of G_{int} were taken as follows: 45.3 $\text{MWm}^{-2}\text{K}^{-1}$ for the PEEK/Graphene, 113.3 $\text{MWm}^{-2}\text{K}^{-1}$ for the PEEK/SiO_2, and 18.0 $\text{MWm}^{-2}\text{K}^{-1}$ for the PEEK/SiC composite, as illustrated in Fig. 3. Besides, the K_{f} values were obtained from our MD simulations with a filler dimension of 6 nm along the heat flow direction. The results were 3.35 $\text{Wm}^{-1}\text{K}^{-1}$ for graphene, 0.9 $\text{Wm}^{-1}\text{K}^{-1}$ for SiO_2, and 5.5 $\text{Wm}^{-1}\text{K}^{-1}$ for SiC.

The influence of ITR on the thermal conductivity of continuous fiber-reinforced composites across varying filler volume fractions ranging from 0 to 0.2 is depicted in Fig. 7. The ratio of K_{eff} to K_{m} is plotted to visualize the thermal property enhancement in PEEK composites. We take a small filler diameter of 6 μm and a large filler length of 1 m to represent the continuous fiber. Three types of continuous fiber were analyzed including carbon fiber (red lines), glass fiber (green lines), and SiC fiber (purple lines). Fig. 7(a) shows that the $K_{\text{eff}}/K_{\text{m}}$ of PEEK composites rises with the increasing filler fraction, and the solid lines which represent the scenario considering the contribution of the interface ($G = G_{\text{int}}$) are overlapped with the dashed lines which represent the scenario neglecting the interface effects ($G = \infty$). This indicates a marginal difference between these two scenarios and the difference is further quantified in Fig. 7(b). It shows that although the relative error in the $K_{\text{eff}}/K_{\text{m}}$ calculation keeps increasing, it remains below 0.01. Additionally, in Fig. 7(a), the slope of $K_{\text{eff}}/K_{\text{m}}$ varies among PEEK composites which are attributed to the differences in the K_{f} values. In particular, the PEEK/SiC composite demonstrates the steepest slope due to the highest K_{f} value of SiC fiber.

The impact of ITR on the thermal conductivity of composites filled with spherical fillers across varying filler volume fractions and diameters is illustrated in Fig. 8. The ratio of K_{eff} to K_{m} is plotted for filler volume fractions ranging from 0 to 0.2, with the filler diameter set to be 10 nm, as shown in Fig. 8(a). Three types of fillers were analyzed including the graphene (red lines), SiO_2 (green lines), and SiC (purple lines). Under the scenario of ideal interfacial contact ($G = \infty$), as presented by the dashed lines, the K_{eff} of composites is expected to increase with the rising filler fractions due to the higher thermal conductivity of filler (K_{f}) compared to that of PEEK, and the rate of this increase is correlated with the values of K_{f}. However, upon accounting for the ITR ($G = G_{\text{int}}$ in solid lines), a significant divergence emerges compared to the dashed lines. For PEEK/SiO_2 (green solid line) and PEEK/graphene (red solid line), a substantial reduction occurs in the rate at which the $K_{\text{eff}}/K_{\text{m}}$ increases with filler fraction. This reduction is attributed to the reduced heat transfer efficiency caused by ITR across the numerous interfaces between the polymer and filler. Intriguingly, for PEEK/SiC composites (purple solid line), $K_{\text{eff}}/K_{\text{m}}$ decreases with the rising filler fraction. Apparently, introducing ITR not only affects the effective thermal conductivity of the composites qualitatively, but also has a significant quantitative impact. As illustrated in Fig. 8(b), the impact of ITR is further quantified by the relative error defined in Eq. (13). The relative error is approximately proportional to the filler volume fraction, with a notably higher escalation rate observed in PEEK/SiC (purple line) compared to PEEK/graphene (red line) and PEEK/SiO_2 (green line). This suggests that the impediment of filler/polymer interfaces to K_{eff} is magnified by a higher filler volume fraction and PEEK/SiC express a higher sensitivity to this effect. Additionally, with the filler volume fraction held constant at 0.2, the effect of filler size was examined for diameters ranging from 3 to 1000 nm. As depicted in Fig. 8(c), the ratio $K_{\text{eff}}/K_{\text{m}}$ under ideal conditions ($G = \infty$ in dashed lines) remains unaffected by variations in filler diameter under the condition of constant filler volume fraction. However, when accounting for the existence of ITR ($G = G_{\text{int}}$), as indicated by the solid lines, the ratio $K_{\text{eff}}/K_{\text{m}}$ is significantly lower at smaller filler diameters compared to the ideal scenario represented by the dashed lines. Then, the ratio increases rapidly and subsequently converges towards the ideal value as the diameter increases. This suggests that

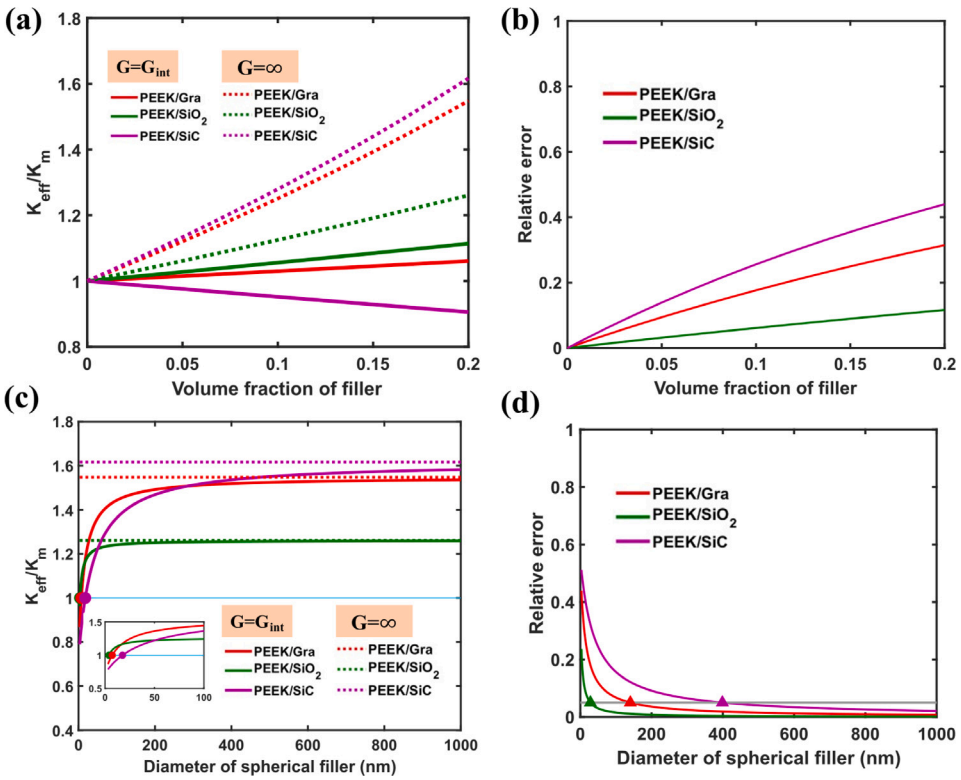

Fig. 8. The influence of interfacial thermal conductivity on PEEK composites filled with spherical graphene, SiO_2, and SiC fillers: (a) The K_{eff}/K_m ratio and (b) relative error in K_{eff} of PEEK composites with respect to varying volume fractions of fillers at a constant filler diameter of 10 nm. (c) The K_{eff}/K_m ratio and (d) relative error in K_{eff} of PEEK composites with varying filler diameters at a fixed filler volume fraction of 0.2. Triangle markers in (c) denote the critical filler sizes where the K_{eff}/K_m ratio, considering ITR, equals 1. The inset in (c) uses the identical coordinate system as the primary plot. In (d), the triangle markers indicate the critical threshold at which the relative error falls below 0.05 for each composite material. (For interpretation of the references to color in this figure legend, the reader is referred to the web version of this article.)

an increase in filler size could substantially mitigate the impact of ITR under the same filler volume fraction. This can be explained by the decreased interfacial contact area within the composite, due to the increased filler size, which reduces the heat loss. Furthermore, the critical filler length were determined at the point where the ratio K_{eff}/K_m reaches 1, as indicated by the light blue line. These critical lengths for different composite systems are marked in Fig. 8(c) by the solid circle markers, with an enlarged view provided in the inset for emphasis. When the filler size is below this critical length, the ratio K_{eff}/K_m is less than one, indicating an adverse effect of the filler on the thermal conductivity of the composite. Conversely, when the filler size exceeds the critical value, the ratio K_{eff}/K_m is greater than one, signifying a positive effect of the filler. For PEEK/graphene, PEEK/SiO_2, and PEEK/SiC composites, the critical filler lengths are determined to be 7.3 nm, 4.0 nm, and 17.7 nm, respectively. These values show an inverse relationship with the G_{int} (Fig. 3) for different PEEK composites. In other words, for composites with higher thermal transport efficiency across the interface, the critical length required for filler to overcome the adverse effect of ITR could become smaller. Furthermore, the relative error in the calculation of K_{eff} is plotted in Fig. 8(d) across a range of filler sizes, exhibiting a rapid decline with increasing filler size. To estimate when the influence of ITR becomes relatively minimal and can be ignored, we set a threshold of 0.05 for the relative error (indicated by the gray line) and identified the threshold length that satisfies this criterion. These threshold lengths are marked with triangles for various composite systems. For PEEK/graphene (red triangle), PEEK/SiO_2 (green triangle) and PEEK/SiC (purple triangle), the relative error falls below 0.05 when the filler diameter surpasses 140.3 nm, 28.4 nm and 398.7 nm, respectively. It can be inferred that this threshold filler diameter increases significantly with a smaller G_{int} of the composite. These findings underscore the role of filler volume fractions and dimensions in influencing the interfacial effects on the thermal properties of composites, particularly for materials with a low G_{int} value.

The thermal properties of composites with flake and cylindrical fillers are also analyzed to assess the impact of filler shape, as shown in Fig. 9. For flake fillers, with a volume fraction of 0.2 and a diameter of 6000 nm, the ratio of K_{eff} to K_m is calculated for lengths from 3 nm to 1000 nm, as illustrated in Fig. 9(a). With the assumption of ideal, perfectly conductive interfaces ($G = \infty$, represented by dashed lines), the ratio K_{eff}/K_m incrementally rises with increasing filler length. In contrast, considering the impact of ITR ($G = G_{int}$, solid lines), the ratio K_{eff}/K_m initially begins at a value that is less than one, then increases sharply, and eventually tends to align with the dashed lines indicative of perfect interfaces. For cylindrical fillers, with a volume fraction of 0.2 and a length of 6000 nm, the variation in the K_{eff} to K_m ratio with filler diameters from 3 nm to 1000 nm is displayed in Fig. 9(b). The ratio K_{eff}/K_m, considering $G = G_{int}$ (solid lines), follows a comparable trend to that in Fig. 9(a), showing an initial steep increase followed by a gradual convergence towards the value represented by $G = \infty$ (dashed lines). Additionally, a critical filler length is identified where $K_{eff}/K_m = 1$ for $G = G_{int}$ for both flake and cylindrical fillers. These critical lengths are summarized in Fig. 9(c) for different filler shapes and materials. It is observed that spherical fillers (blue diamonds), flake fillers (red circles), and cylindrical fillers (yellow triangles) have identical critical sizes of 7.3 nm, 4.0 nm, and 17.7 nm for PEEK/graphene, PEEK/SiO_2, and PEEK/SiC composites, respectively. This indicates that the critical length is independent of the filler shape, but associated with the intrinsic material properties. Furthermore, the relative errors for flake and cylindrical fillers are calculated and depicted in Figs. 9(d) and 9(e), respectively. Both types of fillers show a rapid decrease in relative error, which then gradually stabilizes near zero. However, they show varying rates of decreasing in relative error and display different sensitivities to the filler size. Fig. 9(f) demonstrates the critical

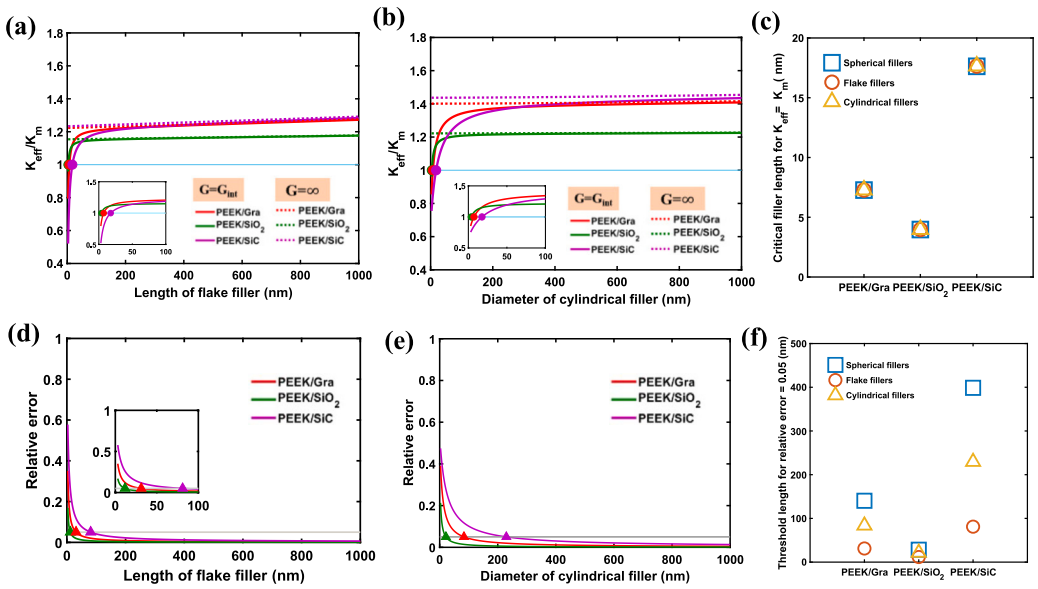

Fig. 9. The influence of interfacial thermal conductivity on composites filled with different shaped fillers: (a) The K_{eff}/K_m ratio for flake fillers at a volume fraction of 0.2 and a diameter of 6 μm, with lengths varying from 3 nm to 1 μm. (b) The K_{eff}/K_m ratio for cylindrical fillers at a volume fraction of 0.2 and a length of 6 μm, with diameters ranging from 3 nm to 1 μm. (c) Critical filler sizes for different filler shapes and materials where the K_{eff}/K_m ratio, considering ITR, equals 1. (d) Relative error in K_{eff} for flake fillers, and (e) relative error in K_{eff} for cylindrical fillers, both at a volume fraction of 0.2. (f) Critical filler thresholds for different filler shapes and materials where the relative error falls below 0.05. The insets in (a) and (d) use the identical coordinate system as their primary plots, respectively. (For interpretation of the references to color in this figure legend, the reader is referred to the web version of this article.)

filler lengths for various shapes at which the relative error reaches 0.05. It can be found that the critical lengths of spherical fillers in composite materials are larger than those of flake and cylindrical fillers. This indicates that nanocomposites filled with spherical fillers can be susceptible to the influence of ITR at a large scale, whereas those with flake fillers are affected only when the filler is reduced to an extremely small scale. Notably, for PEEK/SiC composites, which exhibit larger interfacial thermal resistance, the variation in critical lengths among different filler shapes is more pronounced compared to PEEK/graphene and PEEK/SiO_2 composites. Thus, for composites with spherical SiC fillers, the significance of ITR is highlighted until a sufficient filler size is achieved. While for nanocomposites with flake and cylindrical fillers, the ITR can generally be ignored unless the filler size is extremely small.

In this section, we investigate the role of ITR on the effective thermal conductivity of PEEK composites, taking into account various filler shapes, sizes, and volume fractions. We utilized the relative error R to quantify the disparity in the thermal properties of composites with and without the consideration of ITR. A higher value of R indicates a more important role of ITR in the thermal analysis and modeling of PEEK composites. For continuous fiber-reinforced composites, the extremely small value of R suggests a negligible effect of ITR on the thermal properties of the composite. In contract, for spherical, flake and cylindrical fillers, the necessity to consider ITR in the thermal analysis of PEEK composites depends on the size and fraction of the filler. The influence of ITR on the thermal transport in composite, as represented by the value of R, can be mitigated by reducing the filler fraction and increasing the filler size. Meanwhile, we define a threshold length for fillers to minimize the effect of ITR to an acceptable level, where the relative error R remains below a specific marginal value. For example, if we set this value to 0.05, it means that considering ITR introduces 5% difference compared to the case without ITR. The gray lines in Fig. 8(d) and Fig. 9(d)(e) indicate this level of relative error, and the corresponding solid triangles indicate the threshold length for PEEK composites with graphene (red triangle), SiO2 (green triangle) and SiC (purple triangle). For PEEK composites with SiC fillers, we find that ITR must be considered when the diameter of the spherical fillers reduces to 0.4 μm, while for flake and cylindrical fillers, this occurs when the size reduce to 0.08 μm and 0.23 μm respectively. In other words, these values can be used as references to determine whether to consider the effect of ITR on theoretical modeling and thermal behavior prediction. Since the relative error for continuous fibers is extremely low, it is not necessary to account for ITR in their case. We note that $R = 5\%$ is decided based on our own experience, and other values can be used depending on the specific accuracy requirements of the application. However, the evaluation strategy described in this work remains applicable.

3.4. Discussion

In the systems discussed in this work, the thermal conductivities of the filler materials are higher than that of the PEEK matrix. In the previous section, we analyzed the impact of polymer/filler interfaces on the effective thermal conductivity of composites. As shown in Fig. 6, the analysis focuses on heat conduction through the shorter dimension of the fillers, which involves the maximum number of interfaces. These interfaces lead to phonon scattering, thereby reducing the heat transport efficiency within the composites. As the filler dimensions decrease, with the same filler fraction, the total contact area between the filler and polymer expands exponentially [49], which could significantly reduces the heat transfer efficiency. We define a critical filler dimension L_c at which the ratio K_{eff}/K_m equals one. When the filler dimension drops below this critical value ($L_f < L_c$), the reduction in heat transfer efficiency would overweigh the thermal conductivity enhancements provided by the fillers over the PEEK matrix. This results in a detrimental effect on the K_{eff} of the composite, where K_{eff} decreases with increasing filler volume fraction. This is also observed in the published work, for instance, Wu et al. [3] demonstrated that for single-layer graphene reinforced PEEK, due to the introduction of ITR, the thermal conductivity of the composite in the out-of-plane direction becomes lower than the PEEK polymer.

The critical filler dimensions L_c have been examined across different filler types, shapes, and volume fractions, as demonstrated in Figs. 8 and 9. It was found that L_c, corresponding to the condition where K_{eff}/K_m equals one, varies among different filler materials but is independent on the filler shape and volume fraction. The value of L_c is related to the Kapitza length L_k of the composite system, which

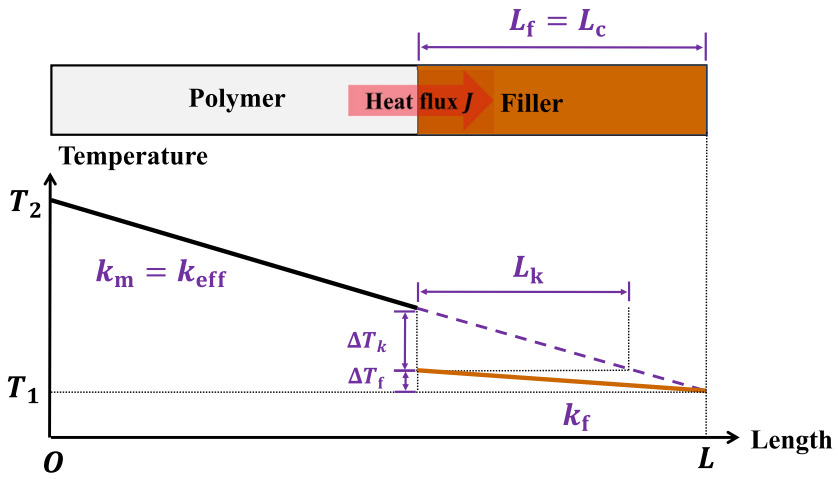

Fig. 10. Illustration of the Kapitza length L_k and critical filler size L_c for $K_{eff}/K_m = 1$.

is given by the formula $L_k = K_m G_{int}^{-1}$ [43]. In Fig. 10, an illustrative plot of the Kapitza length L_k and the critical filler dimension L_c is provided. When the heat flux goes from the polymer to the filler, the temperature experiences a significant drop across the polymer/filler interface, denoted as ΔT_k. The equivalent temperature drop would occur when the heat goes through a polymer region of length L_k, which is the Kapitza length. Additionally, within the filler region, a temperature drop of ΔT_f is observed over a length of L_f. Consequently, in the composite, a total temperature drop $\Delta T_f + \Delta T_k$ occurs with the introduction of the filler. When the dimension of the filler L_f equals L_c, this total temperature drop is equivalent to that in a pure polymer region with the same dimension. This implies that the filler of this size (L_c) neither enhances nor reduces the thermal conductivity of the polymer, which means $K_{eff} = K_m$. From Fig. 10, the relationship between L_c and L_k is numerically derived as follows: $L_c = L_k \frac{K_f}{K_f - K_m}$ (a detailed derivation can be found in supplementary note 4). Utilizing the results from our MD simulation, the L_k are calculated to be 6.6 nm for PEEK/graphene, 2.6 nm for PEEK/SiO_2, and 16.7 nm for PEEK/SiC. These values lead to the respective critical lengths L_c of 7.25 nm, 3.9 nm, and 17.6 nm, which are consistent with the results in Fig. 9(c). They provide a rough guideline that when filler diameters exceed these critical values, interfacial effects should be incorporated into the thermal simulation and analysis of PEEK composites.

Once the filler dimension exceeds L_c, the incorporation of high thermal conductivity fillers can enhance the thermal conductivity of PEEK composites. However, the presence of ITR may significantly reduce the extent of this enhancement. This reduction effect can be quantified using the relative error calculation presented in Eq. (13), where a minimal relative error indicates a negligible interface impact. To constrain the relative error within a specific minor range, the filler dimension should exceed a critical threshold, as indicated by the triangle markers in Figs. 8(d) and 9(d), (e). We note that the threshold value may vary depending on the application requirement. The determination of the critical filler dimension L_c and the critical threshold for minimal relative error could provide guidance for assessing the necessity of incorporating ITR in the analysis of thermal transport phenomena. By integrating the effects of ITR into thermal transport analysis, we can not only optimize the thermal properties of the composite materials but also significantly enhance the accuracy of thermal simulations.

4. Conclusions

In this study, a NEMD approach combined with NAN's theory are employed to investigate the heat transfer performance of various types of PEEK composites. The results highlight that PEEK/SiO_2 and PEEK/graphene demonstrate superior interfacial thermal transport capacity than PEEK/SiC. This improved performance can be attributed to a higher degree of overlap in phonon vibration modes at the interface. Besides, the interfacial thermal resistance may diminish the effective thermal conductivity of composite materials. This reduction can be exacerbated by higher filler volume fractions, smaller filler sizes, spherical filler shapes, and lower interfacial thermal conductivity. Furthermore, we proposed a critical filler length to assess the impact of interfacial thermal resistance and clarified the competitive mechanisms that govern the effective thermal conductivity of PEEK composites. By delving into the significance of interfacial thermal resistance, this study not only contributes to a better understanding of heat transfer mechanism within PEEK composites but also paves the way for multi-scale evaluation of ITR effect and design strategy for efficient thermal management in industries where these materials are prevalent.

Glossary

composite A combination of two or more materials with different physical and chemical properties.

PEEK Poly ether ether ketone.

interfacial thermal resistance The opposition to heat flow across the interface between two materials.

molecular dynamics A computational simulation method used to study the physical movements of atoms and molecules over time.

effective medium theory A theoretical framework used to describe how the properties of composite materials can be understood based on the individual properties of their constituent materials.

phonon A quantum of vibrational energy (as in a crystal).

phonon density of states The number of phonon modes at different frequencies in a crystal.

CRediT authorship contribution statement

Siqin Liu: Writing – original draft, Visualization, Software, Methodology. **Yanan Zhang:** Resources, Funding acquisition. **Xin Yan:** Writing – review & editing, Supervision, Resources, Project administration, Methodology, Data curation, Conceptualization. **Wuxiang Zhang:** Resources. **Xilun Ding:** Resources.

Declaration of Generative AI and AI-assisted technologies in the writing process

During the preparation of this work, the authors used ChatGPT 3.5 in order to enhance the readability of the paper. After using this tool, the authors reviewed and edited the content as needed and took full responsibility for the content of the publication.

Declaration of competing interest

The authors declare that they have no known competing financial interests or personal relationships that could have appeared to influence the work reported in this paper.

Acknowledgments

Funding: This work was supported by the National Natural Science Foundation of China (NSFC, 12372106), the Fundamental Research Funds for the Central Universities, China, the Key Fund Projects of China Academy of Railway Sciences (2022YJ320), and Innovation Research Foundation of COMAC-BUAA Aircraft Research Institute, China (24010209). We acknowledge Information Office of Beihang University for the supply of High Performance Computing Platform. We express our gratitude for the insightful guidance provided by Professor Yaxian Wang from the Chinese Academy of Sciences in our analysis of phonon vibrations.

Appendix A. Supplementary data

Supplementary material related to this article can be found online at https://doi.org/10.1016/j.ijheatmasstransfer.2025.127037.

Data availability

Data will be made available on request.

References

[1] R. Hsissou, R. Seghiri, Z. Benzekri, M. Hilali, M. Rafik, A. Elharfi, Polymer composite materials: A comprehensive review, Compos. Struct. 262 (2021) 113640.
[2] M. Thiruchitrambalam, D.B. Kumar, D. Shanmugam, M. Jawaid, A review on PEEK composites–Manufacturing methods, properties and applications, Mater. Today: Proc. 33 (2020) 1085–1092.
[3] Y. Wu, Y. Liu, L. Zhong, W. Teng, M. Wang, P. Xue, H. Zhang, L. Pan, Molecular dynamics simulation of the effect of functionalization on thermal conductivity of graphene/PEEK composites, Heat Transfer Res. 53 (16) (2022) 1–17.
[4] Z.X. Zhang, S.K. Yang, J.W. Shen, J. Yang, J. Bian, A.P. Zhang, H.L. Lin, D.Q. Chen, Enhanced mechanical, thermal and dielectric properties of polyimide nanocomposites containing SiCp (SiCw) nanofillers for high energy-storage applications, J. Polym. Res. 29 (11) (2022) 444.
[5] J.-M. Park, D.-S. Kim, The influence of crystallinity on interfacial properties of carbon and SiC two-fiber/polyetheretherketone (PEEK) composites, Polym. Compos. 21 (5) (2000) 789–797.
[6] L. Lin, A.K. Schlarb, Development and optimization of high-performance PEEK/CF/Nanosilica hybrid composites, Polym. Adv. Technol. 32 (8) (2021) 3150–3159.
[7] R. Goyal, K. Rokade, A. Kapadia, B. Selukar, B. Garnaik, PEEK/SiO 2 composites with high thermal stability for electronic applications, Electron. Mater. Lett. 9 (2013) 95–100.
[8] J. Njuguna, K. Pielichowski, S. Desai, Nanofiller-reinforced polymer nanocomposites, Polym. Adv. Technol. 19 (8) (2008) 947–959.
[9] Y. Guo, K. Ruan, X. Shi, X. Yang, J. Gu, Factors affecting thermal conductivities of the polymers and polymer composites: A review, Compos. Sci. Technol. 193 (2020) 108134.
[10] C. Wu, F. Xu, H. Wang, H. Liu, F. Yan, C. Ma, Manufacturing technologies of polymer composites—A review, Polymers 15 (3) (2023) 712.
[11] A.K. Roy, B.L. Farmer, V. Varshney, S. Sihn, J. Lee, S. Ganguli, Importance of interfaces in governing thermal transport in composite materials: modeling and experimental perspectives, ACS Appl. Mater. & Interfaces 4 (2) (2012) 545–563.
[12] H. Chen, V.V. Ginzburg, J. Yang, Y. Yang, W. Liu, Y. Huang, L. Du, B. Chen, Thermal conductivity of polymer-based composites: Fundamentals and applications, Prog. Polym. Sci. 59 (2016) 41–85.
[13] T. Zhou, Y. Zhao, Z. Rao, Fundamental and estimation of thermal contact resistance between polymer matrix composites: A review, Int. J. Heat Mass Transfer 189 (2022) 122701.
[14] K. Ruan, X. Shi, Y. Guo, J. Gu, Interfacial thermal resistance in thermally conductive polymer composites: a review, Compos. Commun. 22 (2020) 100518.
[15] T. Luo, J.R. Lloyd, Enhancement of thermal energy transport across graphene/graphite and polymer interfaces: a molecular dynamics study, Adv. Funct. Mater. 22 (12) (2012) 2495–2502.
[16] Y. Li, S. Wang, Q. Wang, Molecular dynamics simulations of thermal properties of polymer composites enhanced by cross-linked graphene sheets, Acta Mech. Solida Sin. 31 (6) (2018) 673–682.
[17] C. Zhao, Y. Tao, Y. Yu, Molecular dynamics simulation of thermal and phonon transport characteristics of nanocomposite phase change material, J. Mol. Liq. 329 (2021) 115448.
[18] Y. Xiong, H. Wu, J. Gao, W. Chen, J. Zhang, Y. Yue, Toward improved thermal conductance of graphene-polyethylene composites via surface defect engineering: a molecular dynamics study, Acta Phys. Chim. Sin 35 (10) (2019) 1150–1156.
[19] V. Varshney, A.K. Roy, J.W. Baur, Modeling the role of bulk and surface characteristics of carbon fiber on thermal conductance across the carbon-fiber/matrix interface, Acs Appl. Mater. & Interfaces 7 (48) (2015) 26674–26683.
[20] M. Wang, Y. Liu, H. Zhang, Y. Wu, L. Pan, Thermal conductivities of Ti3C2Tx MXenes and their interfacial thermal performance in MXene/epoxy composites–a molecular dynamics simulation, Int. J. Heat Mass Transfer 194 (2022) 123027.
[21] Z. Wang, Z. Cheng, D. Chen, B. Yao, M. An, Enhancement of interfacial thermal conductance at semiconductor/polymer interfaces induced by intercalating water layer in humidity environment, Int. J. Heat Mass Transfer 239 (2025) 126495, http://dx.doi.org/10.1016/j.ijheatmasstransfer.2024.126495, URL https://www.sciencedirect.com/science/article/pii/S0017931024013231.
[22] L. Song, Y. Zhang, J. Zhan, Y. An, W. Yang, J. Tan, L. Cheng, Interfacial thermal resistance in polymer composites: a molecular dynamic perspective, Mol. Simul. 48 (10) (2022) 902–925.
[23] Q. Zhang, Y. Chen, Y. Zhang, J. Sun, M. Hu, X. Yan, K. Yuan, X. Yang, J. Li, Surface oxidation modulates the interfacial and lateral thermal migration of MXene (Ti3C2T x) flakes, J. Phys. Chem. Lett. 11 (22) (2020) 9521–9527.
[24] M. Hassanzadeh-Aghdam, M. Mahmoodi, J. Jamali, Effect of CNT coating on the overall thermal conductivity of unidirectional polymer hybrid nanocomposites, Int. J. Heat Mass Transfer 124 (2018) 190–200, http://dx.doi.org/10.1016/j.ijheatmasstransfer.2018.03.065, URL https://www.sciencedirect.com/science/article/pii/S0017931018306987.
[25] X. Wang, X. Niu, X. Wang, X. Qiu, L. Wang, Effects of filler distribution and interface thermal resistance on the thermal conductivity of composites filling with complex shaped fillers, Int. J. Therm. Sci. 160 (2021) 106678, http://dx.doi.org/10.1016/j.ijthermalsci.2020.106678, URL https://www.sciencedirect.com/science/article/pii/S1290072920311273.
[26] N. Siraj, S.A.R. Hashmi, S. Verma, State-of-the-art review on the high-performance poly (ether ether ketone) composites for mechanical, tribological and bioactive characteristics, Polym. Adv. Technol. 33 (10) (2022) 3049–3077.
[27] J. Njuguna, F. Ansari, S. Sachse, V.M. Rodriguez, S. Siqqique, H. Zhu, 1 - nanomaterials, nanofillers, and nanocomposites: types and properties, in: J. Njuguna, K. Pielichowski, H. Zhu (Eds.), Health and Environmental Safety of Nanomaterials (Second Edition), second ed., in: Woodhead Publishing Series in Composites Science and Engineering, Woodhead Publishing, 2021, pp. 3–37, http://dx.doi.org/10.1016/B978-0-12-820505-1.00011-0, URL https://www.sciencedirect.com/science/article/pii/B9780128205051000110.
[28] D. Khater, F. Odeh, W. Alahmad, M. Alkhabbas, R. Afaneh, A. Al Bawab, M.S. Mubarak, Nanoparticles and nanofillers: Types, methods of preparation and characterization, and safety, in: S. Mallakpour, C.M. Hussain (Eds.), Handbook of Nanofillers, Springer Nature Singapore, Singapore, 2025, pp. 1–44, http://dx.doi.org/10.1007/978-981-99-3516-1_4-1.
[29] P. Wang, B. Zou, S. Ding, C. Huang, Z. Shi, Y. Ma, P. Yao, Preparation of short CF/GF reinforced PEEK composite filaments and their comprehensive properties evaluation for FDM-3D printing, Compos. Part B: Eng. 198 (2020) 108175.
[30] A.P. Thompson, H.M. Aktulga, R. Berger, D.S. Bolintineanu, W.M. Brown, P.S. Crozier, P.J. in't Veld, A. Kohlmeyer, S.G. Moore, T.D. Nguyen, R. Shan, M.J. Stevens, J. Tranchida, C. Trott, S.J. Plimpton, LAMMPS - a flexible simulation tool for particle-based materials modeling at the atomic, meso, and continuum scales, Comput. Phys. Comm. 271 (2022) 108171.
[31] Y. Yan, J. Xu, H. Zhu, Y. Xu, M. Wang, B. Wang, C. Yang, Molecular dynamics simulation of the interface properties of continuous carbon fiber/polyimide composites, Appl. Surf. Sci. 563 (2021) 150370.
[32] M. Zhang, B. Jiang, C. Chen, D. Drummer, Z. Zhai, The effect of temperature and strain rate on the interfacial behavior of glass fiber reinforced polypropylene composites: a molecular dynamics study, Polymers 11 (11) (2019) 1766.
[33] X.Q. Wang, D. Lau, Atomistic investigation of GFRP composites under chloride environment, Adv. Struct. Eng. 24 (6) (2021) 1138–1149.
[34] A. Salinas, M. Lizcano, K. Lozano, Synthesis of β-SiC fine fibers by the forcespinning method with microwave irradiation, J. Ceram. 2015 (2015) 1–5.

[35] H. Sun, S.J. Mumby, J.R. Maple, A.T. Hagler, An ab initio CFF93 all-atom force field for polycarbonates, J. Am. Chem. Soc. 116 (7) (1994) 2978–2987.
[36] P. Zhang, J. Zeng, S. Zhai, Y. Xian, D. Yang, Q. Li, Thermal properties of graphene filled polymer composite thermal interface materials, Macromol. Mater. Eng. 302 (9) (2017) 1700068.
[37] S.J. Stuart, A.B. Tutein, J.A. Harrison, A reactive potential for hydrocarbons with intermolecular interactions, J. Chem. Phys. 112 (14) (2000) 6472–6486.
[38] S. Munetoh, T. Motooka, K. Moriguchi, A. Shintani, Interatomic potential for Si–O systems using Tersoff parameterization, Comput. Mater. Sci. 39 (2) (2007) 334–339.
[39] J. Tersoff, Modeling solid-state chemistry: Interatomic potentials for multicomponent systems, Phys. Rev. B 39 (8) (1989) 5566.
[40] M. Waldman, A.T. Hagler, New combining rules for rare gas van der Waals parameters, J. Comput. Chem. 14 (9) (1993) 1077–1084.
[41] S. Wang, X. Yan, B. Chang, S. Liu, L. Shao, W. Zhang, Y. Zhu, X. Ding, Atomistic modeling of the effect of temperature on interfacial properties of 3D-printed continuous carbon fiber-reinforced polyamide 6 composite: From processing to loading, ACS Appl. Mater. & Interfaces 15 (48) (2023) 56454–56463, http://dx.doi.org/10.1021/acsami.3c12372.
[42] M. Nikonovich, J.F. Costa, A.C. Fonseca, A. Ramalho, N. Emami, Structural, thermal, and mechanical characterisation of PEEK-based composites in cryogenic temperature, Polym. Test. 125 (2023) 108139.
[43] J. Chen, X. Xu, J. Zhou, B. Li, Interfacial thermal resistance: Past, present, and future, Rev. Modern Phys. 94 (2) (2022) 025002.
[44] A. Cao, J. Qu, Kapitza conductance of symmetric tilt grain boundaries in graphene, J. Appl. Phys. 111 (5) (2012) 053529.
[45] T. Luo, J.R. Lloyd, Non-equilibrium molecular dynamics study of thermal energy transport in Au–SAM–Au junctions, Int. J. Heat Mass Transfer 53 (1–3) (2010) 1–11.
[46] L. Zhang, L. Liu, Hierarchically hydrogen-bonded graphene/polymer interfaces with drastically enhanced interfacial thermal conductance, Nanoscale 11 (2019) 3656–3664.
[47] C.-W. Nan, R. Birringer, D.R. Clarke, H. Gleiter, Effective thermal conductivity of particulate composites with interfacial thermal resistance, J. Appl. Phys. 81 (10) (1997) 6692–6699.
[48] R. Knibbs, The use of polarized light microscopy in examining the structure of carbon fibres, J. Microsc. 94 (3) (1971) 273–281.
[49] T. Evgin, H.D. Koca, N. Horny, A. Turgut, I.H. Tavman, M. Chirtoc, M. Omastová, I. Novak, Effect of aspect ratio on thermal conductivity of high density polyethylene/multi-walled carbon nanotubes nanocomposites, Compos. Part A: Appl. Sci. Manuf. 82 (2016) 208–213.